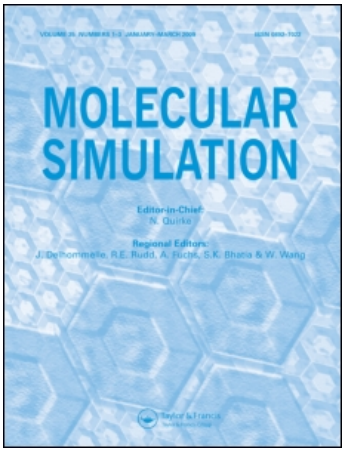

Molecular Simulation

Publication details, including instructions for authors and subscription information:
http://www.informaworld.com/smpp/title~content=t713644482

Uncertainty and figure selection for DFT based cluster expansions for oxygen adsorption on Au and Pt (111) surfaces

Spencer D. Miller[a]; John R. Kitchin[a]
[a] Department of Chemical Engineering, Carnegie Mellon University, Pittsburgh, PA, USA

To cite this Article Miller, Spencer D. and Kitchin, John R.(2009) 'Uncertainty and figure selection for DFT based cluster expansions for oxygen adsorption on Au and Pt (111) surfaces', Molecular Simulation, 35: 10, 920 — 927
To link to this Article: DOI: 10.1080/08927020902833137
URL: http://dx.doi.org/10.1080/08927020902833137

Molecular Simulation
Vol. 35, Nos. 10–11, September 2009, 920–927

Taylor & Francis
Taylor & Francis Group

Uncertainty and figure selection for DFT based cluster expansions for oxygen adsorption on Au and Pt (111) surfaces

Spencer D. Miller and John R. Kitchin*

Department of Chemical Engineering, Carnegie Mellon University, Pittsburgh, PA 15213, USA

(*Received 15 December 2008; final version received 16 February 2009*)

We utilise two-dimensional cluster expansions in order to extend a small density functional theory (DFT) database of oxygen adsorption energies on Au and Pt (111) surfaces to explore a wide range of configurational space in larger unit cells than can be conveniently examined by DFT. We calculate adsorption energies and heats of formation for all configurations of up to 15 adsorption sites using the cluster expansions. We show how the cluster expansion adsorption energies obey the configurational correlation previously observed for the DFT results. The ramifications of figure selection are considered and the use of cross-validation scores to weigh figure sets and determine predictive power is examined. Finally, we show that there are only a small number of structural motifs needed to describe the most relevant structures in the phase diagram on these metals.

Keywords: density functional calculations; adsorption; cluster expansions; oxygen; platinum; gold

1. Introduction

Coverage dependence of adsorption properties can play an important role in many reactions that occur on catalytic surfaces. One widely deployed method for studying such coverage dependence is density functional theory (DFT). Oxygen is a widely considered adsorbate for such studies and has been studied on many transition metals such as platinum [1–4], ruthenium [5], rhodium [6], palladium [7,8], gold [4,9], and copper [10]. Other adsorbates have also been considered such as sulphur on Cu, Ag, and Pd [11,12], and nitrogen on Ru [13] and Cu [14,15].

One goal in computational surface science is to predict phase behaviour and to identify low energy, i.e. stable surface structures. One limitation of DFT is that it is very expensive in terms of computational resources, limiting the number of configurations that can be reasonably calculated. Consequently, there is often uncertainty about whether there exist other, lower energy configurations than the set considered. Cluster expansions can be used in order to extend DFT results to a far wider range of configurations, thus increasing the probability of identifying relevant configurations. Three-dimensional cluster expansions have been widely used in studies of bulk alloy systems, and more recently the cluster expansion has found applications in a two-dimensional form for the study of surface adsorption systems [2,16–20].

In this application the adsorption system is coarse-grained to an Ising lattice model, where each adsorption site (typically the fcc site on a (111) surface) is represented as a single lattice point. The occupancy of each lattice point is then represented by a spin variable (σ), for example it can be set so that spin up ($+1$) corresponds to an occupied site and spin down (-1) corresponds to a vacant site. The cluster expansion results should be independent of spin value selection provided that the expansion is based on a complete figure basis set, this means that the set also includes all sub-figures of every figure included in the set [21].

In this work we will present the results of cluster expansions on a set of DFT data presented in detail elsewhere [4]. This will include a detailed look at the method we employ for the selection of the basis set of figures, and the potential ramifications of figure selection on the cluster expansion results. We also return to the configurational correlation previously identified through our DFT results and show that it is consistent with the cluster expansion. Additionally we utilise the cluster expansion to produce phase diagrams based on heats of formation, and study the structural similarity of those thermodynamically stable configurations that lie near the convex hulls.

2. Methods

The DFT calculation basis set utilised in this study [4] was calculated using first-principles DFT as implemented in the Vienna *Ab initio* Simulations Package [22–25]. All calculations were performed using the projector augmented wave method [26] and the gradient-corrected Perdew-Wang 91 (PW91-GGA) exchange-correlation functional

*Corresponding author. Email: jkitchin@andrew.cmu.edu

ISSN 0892-7022 print/ISSN 1029-0435 online

DOI: 10.1080/08927020902833137
http://www.informaworld.com

[27], without symmetry reduction. Only the oxygen molecule in a box was calculated with spin polarisation. Cut-off energies of 425 eV for platinum slabs and 475 eV for gold were used in the final calculations. *k*-point densities equating to 12 × 12 × 1 *k*-points for a 1 × 1 surface unit cell were used for the final calculations in both cases, using the Monkhorst-Pack grid [28]. All adsorption energies were calculated with reference to the energies of clean surfaces calculated with commensurate *k*-point grids. The final platinum adsorption energies were found to be converged to about 0.02 eV/O, and on gold to 0.03 eV/O.

Five layer (111) slabs were used for all calculations, with the bottom three layers fixed in bulk positions, with adsorbed oxygen atoms placed only on the relaxed 'upper' side of the slab. A vacuum space of five layers (corresponding to more than 10 Å) separated the slabs to prevent any interactions between the periodically repeated slabs. A lattice constant of 4.18 Å was used for gold, and 4.00 Å for platinum which are comparable to both experimental and computational values [1,9].

Adsorption energies were calculated on a per adsorbate basis with reference to molecular oxygen as shown in Equation (1).

$$\Delta H_{\text{ads}} = \frac{E_{\text{M-O}} - E_{\text{M}} - N_{\text{O}} \cdot (1/2) E_{\text{O}_2}}{N_{\text{O}}} \tag{1}$$

ΔH_{ads} is the adsorption energy, $E_{\text{M-O}}$ is the total energy of the metal slab with adsorbed oxygen, E_{M} is the energy of the clean metal surface, N_{O} is the number of oxygen atoms adsorbed on the surface, and E_{O_2} is the energy of a single oxygen molecule in vacuum. In this convention, negative adsorption energies are exothermic and thermodynamically favourable with respect to gas phase, molecular oxygen. The two-dimensional cluster expansion was utilised in order to expand our results to configurations whose adsorption energies were not directly calculated using DFT. The cluster expansion is similar to other expansions such as those using the Taylor series, or Fourier series. In the case of a cluster expansion the basis set of polynomials are known as 'figures' and the set is both complete and orthogonal, meaning that the expansion is exact in the limit of an infinite basis set [29]. The cluster expansion assumes an Ising lattice model [30] where each adsorption site is represented by a lattice point that is either spin up (occupied, $\sigma = 1$) or spin down (unoccupied $\sigma = -1$). The basis functions α are polynomials in spin products over all the vertices ν within a figure for a given site (Equation (2)). The basis functions are summed and averaged over each site in the configuration to yield Π_α for a particular figure α (Equation (3)). Finally, each symmetry and translationally equivalent figure to α is collected in a set of figures F and the average value of the set of Π_α is calculated in Equation (4). The correlation vector, Π_α, is the mathematical representation of the configuration used in the cluster expansion.

$$\pi_{\alpha,\text{site}} = \frac{1}{\nu_\alpha} \prod_{i=1}^{\nu_\alpha} \sigma_i \tag{2}$$

$$\Pi_\alpha = \frac{1}{N_{\text{sites}}} \sum_{j=1}^{N_{\text{sites}}} \pi_{\alpha,j} \tag{3}$$

$$\bar{\Pi}_F = \frac{\nu_\alpha}{N_F} \sum_{k=1}^{N_F} \Pi_{F_k}. \tag{4}$$

Equation (2) is a product of all spin variables for a given figure α on a given site, and ν_α is the number of sites or vertices in the figure. Equation (3) is a sum over all sites in a given configuration divided by the total number of sites on the configuration, and Equation (4) is the sum over all symmetrically equivalent figures which produces the correlation value for that figure on that configuration. The vector of these values for every figure set in the expansion basis set is the correlation vector, $\bar{\Pi}$, for the configuration. These correlation vectors can be constructed as a matrix of vectors $\underline{\underline{\Pi}}$, one for each configuration considered, and are then used in the final cluster expansion equation (Equation (5)).

$$\underline{E} = \underline{\underline{\Pi}} \cdot \underline{J} \tag{5}$$

where $\underline{E}$ is the vector of energies calculated using DFT, and $\underline{J}$ is the vector of expansion coefficients. In order to use the expansion it is necessary to determine the expansion coefficients $\underline{J}$. These can be fitted using a least squares algorithm from the known DFT energies, and the correlation vectors for each configuration. Once the expansion coefficients are known it is then possible to calculate the energy of any adsorbate configuration by calculating its correlation vector and multiplying this by $\underline{J}$.

While the set of figures which forms the basis set for the cluster expansion is exact in the infinite limit; for any practical application the set must be truncated at a finite limit. We utilised a set of 18 figures in our basis set to choose from, including zero, one, two, three, and four vertex figures – these are shown in Figure 1. The challenge

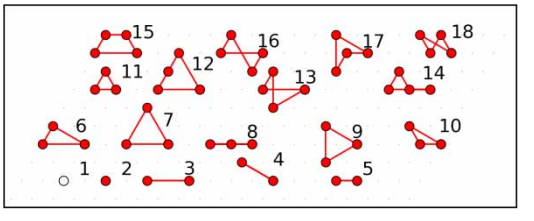

Figure 1. Schematic of figures made available for the cluster expansions presented in this paper. Red circles represent the lattice points covered by the figure.

in fitting cluster expansions is selecting a set of figures that accurately and faithfully reproduces the set of DFT results. Too few figures will not fit the data adequately, whereas too many could overfit the data and lead to unreliable predictions.

The purpose of the cluster expansion is to make accurate predictions for the adsorption energies of configurations for which DFT calculations are not available. Therefore, we weigh the accuracy of the cluster expansion in terms of its predictive power. Prediction errors were calculated by leaving one or more DFT configurations out of the set of configurations used to fit $\underline{J}$, and then comparing the energy predicted for that configuration by the cluster expansion to the calculated DFT value.

This process was then repeated for every possible leave one out, leave two out and leave three out scenario, to provide a very large set of prediction errors which could then be averaged over to produce the CV score as shown in Equation (6). M is the total number of cluster expansion energy predictions made, $E^{\text{predicted}}$ is the energy calculated by the cluster expansion for a given fit and configuration i, and E^{DFT} is the energy of that configuration as calculated by DFT

$$\text{CV}_{\text{score}} = \sqrt{\frac{1}{M}\sum_{i=1}^{M}\left(E_i^{\text{predicted}} - E_i^{\text{DFT}}\right)^2}. \qquad (6)$$

$$\kappa(\Pi) = \frac{s_{\max}\left(\underline{\underline{\Pi}}\right)}{s_{\min}\left(\underline{\underline{\Pi}}\right)}. \qquad (7)$$

This procedure presents one notable weakness. Due to the similarity of some configurations it was possible to produce correlation matrices with determinants near zero, that is strongly ill-conditioned matrices. This results in very unstable $\underline{J}$ vectors and large prediction errors. In order to avoid this shortfall, any $\underline{J}$'s fit to ill-conditioned correlation matrices $\left(\underline{\underline{\Pi}}\right)$ as defined by those with condition numbers (κ) in excess of 1000 as calculated by Equation (7) (where the $s\left(\underline{\underline{\Pi}}\right)$'s refer to the minimal and maximal singular values of the correlation matrix), were ignored for the purposes of calculating the cross-validation score. One result of this procedure was to produce more reliable CV scores, but another was that the number of errors over which the CV score is calculated was no longer the same for every figure set, due to differences in how many ill-conditioned correlation matrices different figure sets produce. Therefore, a minimum number of errors must be set for consideration of a figure set, which we set to be 6000. In addition to excluding those figure sets which produce many ill-conditioned correlation matrices, this condition also ruled out very large figure sets. This is due

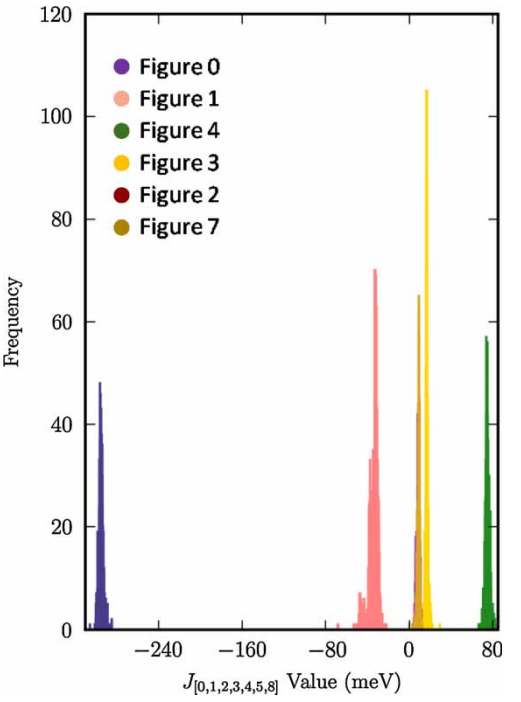

Figure 2. Distribution of $\underline{J}$ values for the lowest CV score figure set on platinum, colour coded for each figure in the figure set as noted in the upper lefthand corner. Figures are listed (from top to bottom) in order of increasing figure size. Notable are the narrow distribution of the $\underline{J}$ values around averages that are either positive or negative. Additionally the magnitude of the average $\underline{J}$ value decreases as figure size increases, demonstrating the trend towards zero for higher order terms of the expansion.

to the inability to produce a fit for a figure set which includes more figures than there are configurations to fit to (under-specification), so those figure sets of 12 or more figures which did not allow for leave-three out fits were also excluded. These figure sets are not expected to be any more accurate than smaller figure sets as discussed later.

This procedure was performed for each possible figure set that could be composed from the 18 figures in Figure 1 within the following constraints. Firstly, all figure sets included Figures 1–5 which are the most simple figures including the zero and one body figures, and the two body nearest neighbour and second nearest neighbour figures. Additionally all figure sets considered were complete [21], that is for each figure included in a figure set, every sub-figure of that figure was also included in the figure set. Every figure set that met these conditions was considered, and a CV score calculated for each.

Heats of formation (ΔH_{F}) were calculated for the purpose of constructing a phase diagram. We did not include the vibrational energy of the adsorbates in these calculations. These heats of formation are a measure of the

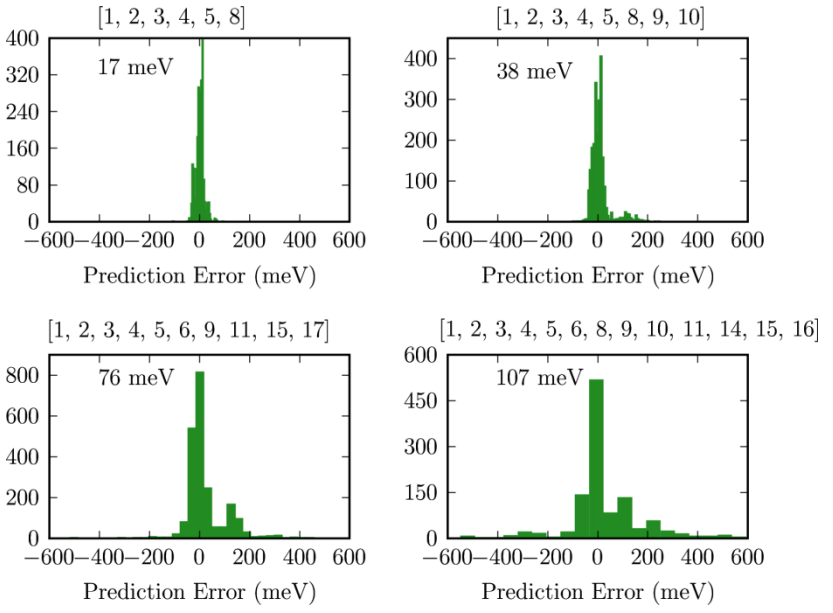

Figure 3. Prediction error distribution plotted for different figure sets with the figure set's CV score noted in the upper left-hand corner. The range and magnitude of the errors increases with the CV score, demonstrating how the CV score serves as a measure of a figure set's prediction error.

relative stability of a given configuration with regards to phase separation between regions of zero coverage and regions of full coverage, as shown in Equation (8). $E_{\mathrm{M-O}}$ is the total energy of the metal slab with adsorbed oxygen, E_{M} is the energy of the clean metal surface, $E_{p(1\times1)-\mathrm{O}}$ is the energy of the slab with a full mono-layer of adsorbed oxygen, and θ is the oxygen coverage of the configuration in question

$$\Delta H_{\mathrm{F}} = E_{\mathrm{M-O}} - (1-\theta)E_{\mathrm{M}} - \theta E_{p(1\times1)-\mathrm{O}}. \qquad (8)$$

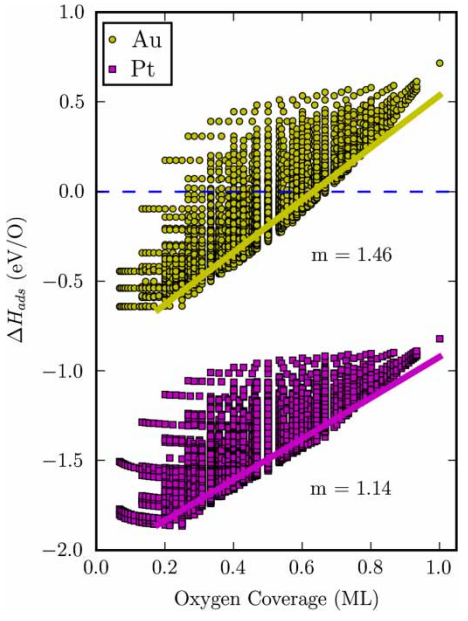

Figure 4. Adsorption energies as calculated by the cluster expansion for gold (yellow) and platinum (magenta). Trend lines for the lowest energy configurations at each coverage are shown with their slopes.

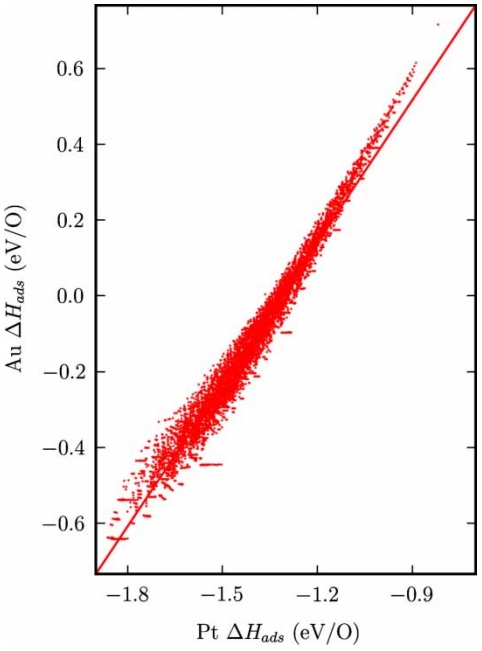

Figure 5. Configurational correlation for the cluster expansion adsorption energies. The line is the best fit line for all data points, suggesting that there may be some nonlinearity in the correlation.

3. Results and discussion

The practical cluster expansion is a truncation of the infinite and exact cluster expansion. For this truncation to be an accurate approximation, it is necessary for the higher order terms of the expansion, corresponding to larger figure sizes, to tend towards zero. If this were not the case, then neglecting the contributions from higher order terms would result in significant errors. In order to show that they do tend towards zero we have plotted the $\underline{J}$ distribution for the figure set on the platinum data which produced the lowest CV score (17 meV). This $\underline{J}$ distribution includes the $\underline{J}$ values for each fit performed in the CV score calculation for this figure set. The distribution of $\underline{J}$'s from the leave one out, two out, and three out fits is shown in Figure 2. Here, it is seen that the $\underline{J}$'s themselves vary in a roughly normal distribution that can either be positive or negative on average. Additionally, the average magnitude of these $\underline{J}$ distributions decreases as the figure size itself increases. This is consistent with the higher order contributions tending towards zero, which means that not only do larger figures (and hence larger figure sets) add relatively little to the results of the cluster expansion, but that the infinite series can be meaningfully represented by a smaller truncated set of basis functions.

In order to show that the CV score provides a meaningful measure of the predictive power of a cluster expansion with a given figure set, we have plotted the distribution of prediction errors for four figure sets with different CV scores. The results are shown in Figure 3. Cluster expansions produced with good figure sets, that is those with low-CV scores, produce a narrow distribution of prediction errors centred around zero. Poor figure sets, those with high-CV scores, however produce prediction errors with both higher error magnitudes as well as a much wider distribution. The width of this distribution is linked to the magnitude of the CV score, figure sets with higher CV scores produce wider distributions. This confirms the principle of the CV score as a measure of predictive error for the cluster expansion based on that figure set. Thus, not only does the calculation of the CV score for each figure set allows for an effective means of weighting them, but it also provides a measure of the cluster expansion's uncertainty.

The results of the DFT calculations for oxygen adsorption on the gold and platinum (111) surfaces were characterised previously in the form of adsorption energies. The adsorption energies were limited to a total of 15 configurations with non-zero coverage. We now use the cluster expansion to expand upon these results to cover a much wider range of configurations. We performed cluster expansions with the best figure sets on each surface to calculate the adsorption energies for every symmetrically and translationally unique configuration in unit cells of up to 15 adsorption sites on the fcc (111) surfaces. The results of these adsorption energy calculations, for 8917 total configurations, are shown in Figure 4. The best fit lines for the lowest energy configurations at each coverage are plotted with their slopes. While the trend of the DFT data appeared roughly linear, there's a noticeable nonlinearity in the cluster expansion adsorption energies suggesting that a linear fit may not fully capture the adsorption energy coverage dependence, especially at high coverage.

We previously observed a configurational correlation among the adsorption energies on Pt(111) and Au(111). The same correlation exists for the cluster expansion adsorption energies as shown in Figure 5. While this may be expected for the lowest energy configurations, which may be roughly linear, and would thus simply be a linear correlation between two linearly correlated functions of coverage, the higher energy configurations also obey the correlation suggesting that a more fundamental relationship, such as the *d*-band adsorption model shared by both systems [4], is responsible for this similarity. The cluster expansion correlation displays some noted asymmetry, which is similar to the asymmetry observed in the adsorption energies.

Heats of formation as defined in Equation (8) provide a measure of the stability of an adsorbate configuration with regard to phase separation into regions of zero coverage and full coverage. Those configurations which are most stable are connected by tie lines, which form what is known as the convex hull. Those configurations found near the convex hull are thus the most thermodynamically relevant configurations. Due to the computational resources requirements of DFT, only a very limited number of configurations can be covered. The cluster expansion, however, allows for the rapid calculation of these heats of formation for all configurations of up to 15 sites, shown in Figure 6 for platinum and Figure 7 for gold.

There is uncertainty in the cluster expansion heats of formation both due to convergence of the DFT data (20 meV for platinum, 30 meV for gold) and due to the uncertainty in the fit of the cluster expansion to this noisy data (approximately 20 meV rms prediction error for both surfaces). This uncertainty makes it difficult to identify which configurations lie on, rather than just near, the convex hull. An alternative and complementary analysis of stability in this context is to examine the structural similarity of neighbouring configurations. If all of the neighbouring configurations share certain structural features it becomes less important to identify exactly which structure is lowest in energy.

The correlation vector for a configuration provides a 'finger print' for the configurational characteristics of that configuration. We can quantify the similarity by calculating the dot product of two correlation vectors and normalizing by the lengths of each vector. This yields a value of 1 for identical configurations, and a value that

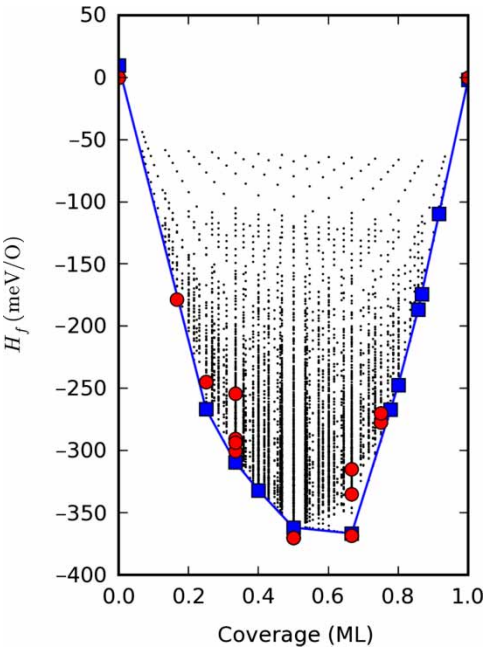

Figure 6. Heats of formation as calculated by the cluster expansion for oxygen adsorption on platinum. The black dots represent the cluster expansion heats of formation, red circles those from DFT calculations, and blue squares are the points along the convex hull which is itself represented by the blue line.

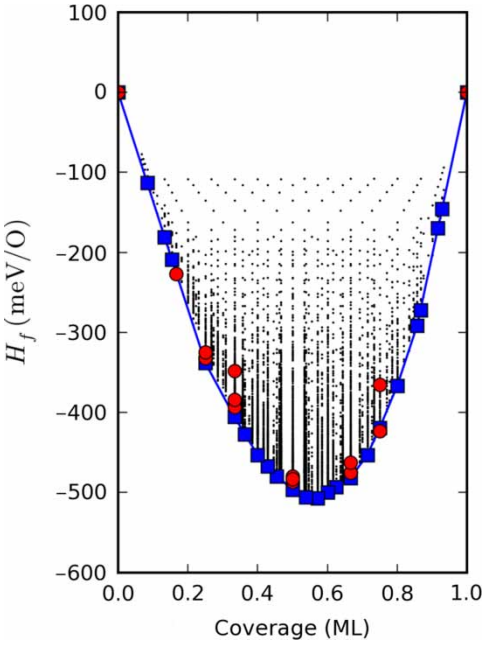

Figure 7. Heats of formation as calculated by the cluster expansion for oxygen adsorption on gold. The black dots represent the cluster expansion heats of formation, red circles those from DFT calculations, and blue squares are the points along the convex hull which is itself represented by the blue line.

approaches zero for completely dissimilar configurations. Seven simple reference configurations were selected from those that appear widely in surface adsorption studies, and for every configuration considered in the cluster expansions, and evaluated the similarity of all the configurations to these configurations in Figure 8 (platinum) and Figure 9 (gold). The similarity is presented as a circle with a radius proportional to the similarity measure described above raised to a power. The exponent is not critical and serves to accentuate the similarity of the configurations by making small similarity measures even smaller. We examined powers in the range of 5–30, with both figures being generated with a power of 30.

On both surfaces those configurations lying near the convex hull are generally very similar to neighbouring configurations. Rather than belonging to a set of widely independent configurations they instead fall into a smaller number of 'thematic' configurational regions, with each configuration in the region being a variation on the reference configuration. This suggests that while we cannot determine with certainty which configurations are in fact the most stable, we can identify which broad configurational theme dominates in each coverage region with confidence. Depending on the particular figure set used for the cluster expansion there is a small region near

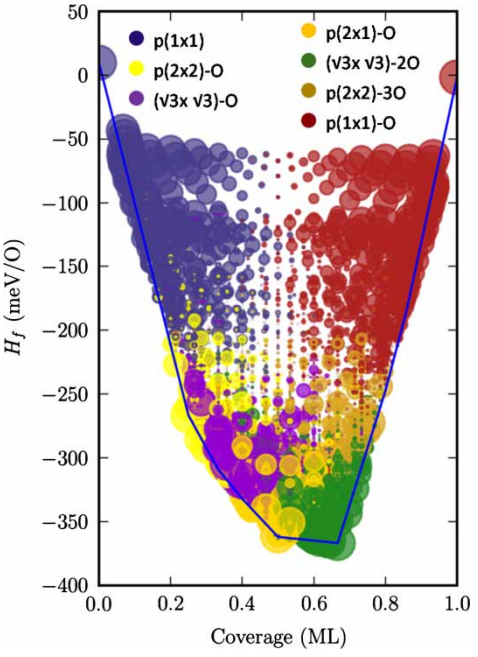

Figure 8. Similarity diagram for the platinum surface. Circles have been plotted for every configuration which show the configuration's similarity to the reference configurations at the top of the figure. The colour of the circle corresponds to the reference configuration, and the radius of the circle is proportional to the configurations similarity to the reference configuration.

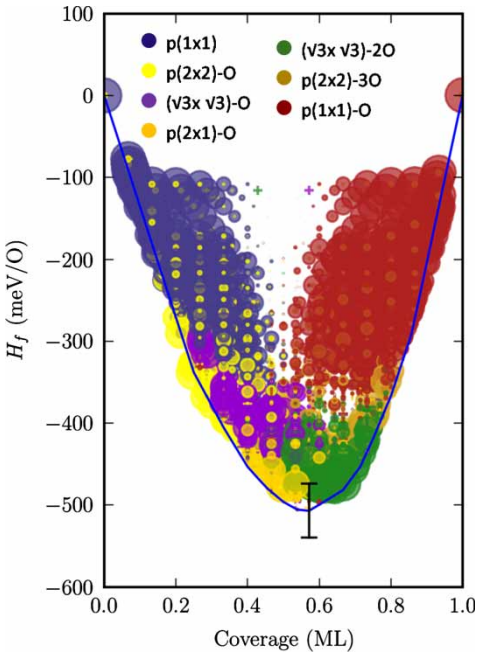

Figure 9. Similarity diagram for the gold surface. The error bar corresponds to the 95% confidence range for the lowest heat of formation configuration, it represents how much uncertainty is present in the ordering of configurations near the convex hull.

0.5 ML on the gold surface where there is no apparent similarity to the reference structures shown. The size of this region is within the uncertainty expected from the cluster expansion, as shown through the error bar, and consequently we cannot reach a reliable conclusion on the relevance of these configurations.

4. Conclusions

We have shown how CV scores can be utilised to weigh the predictive power of a cluster expansion, and to select a figure basis set for use in the expansion. We have then utilised the cluster expansion to calculate adsorption energies, which we found to be consistent with DFT results. As previously observed with DFT, the full configuration space of adsorption energies were correlated to one another. Additionally we calculated heats of formation for both surfaces and showed how the configurations which lie near the convex hull are not completely independent but instead fall into a rather limited set of configurations in the region near the convex hull.

Acknowledgements

Funding is gratefully acknowledged from the Department of Energy Office of Basic Energy Science (Grant DOE-BES DEFG0207ER15919).

References

[1] H.R. Tang, A. Van der Ven, and B.L. Trout, *Phase diagram of oxygen adsorbed on platinum (111) by first-principles investigation*, Phys. Rev. B 70 (2004), 045420.
[2] H.R. Tang, A. Van der Ven, and B.L. Trout, *Lateral interactions between oxygen atoms adsorbed on platinum (111) by first principles*, Mol. Phys. 102 (2004), pp. 273–279.
[3] R.B. Getman, Y. Xu, and W.F. Schneider, *Thermodynamics of environment-dependent oxygen chemisorption on Pt(111)*, J. Phys. Chem. C 112 (2008), pp. 9559–9572.
[4] S.D. Miller and J.R. Kitchin, *Relating the coverage dependence of oxygen adsorption on Au and Pt fcc(111) surfaces through adsorbate-induced surface electronic structure effects*, Surf. Sci. (2009), doi: 10.1016/j.susc.2009.01.021, in print.
[5] C. Stampfl and M. Scheffler, *Density-functional theory study of the catalytic oxidation of CO over transition metal surfaces*, Surf. Sci. 435 (1999), pp. 119–126.
[6] O.R. Inderwildi, D. Lebiedz, O. Deutschmann, and J. Warnatz, *Coverage dependence of oxygen decomposition and surface diffusion on rhodium (111): a DFT study*, J. Chem. Phys. 122 (2005), 034710.
[7] Y.S. Zhang, V. Blum, and K. Reuter, *Accuracy of first-principles lateral interactions: Oxygen at Pd(100)*, Phys. Rev. B 75 (2007), 235406.
[8] M. Todorova, K. Reuter, and M. Scheffler, *Oxygen overlayers on Pd(111) studied by density functional theory*, J. Phys. Chem. B 108 (2004), pp. 14477–14483.
[9] H. Shi and C. Stampfl, *First-principles investigations of the structure and stability of oxygen adsorption and surface oxide formation at Au(111)*, Phys. Rev. B 76 (2007), 075327.
[10] A. Soon, M. Todorova, B. Delley, and C. Stampfl, *Oxygen adsorption and stability of surface oxides on Cu(111): a first-principles investigation*, Phys. Rev. B 73 (2006), 165424.
[11] M. May, S. Gonzalez, and F. Illas, *A systematic density functional study of ordered sulfur overlayers on Cu(111) and Ag(111): influence of the adsorbate coverage*, Surf. Sci. 602 (2008), pp. 906–913.
[12] D.R. Alfonso, A.V. Cugini, and D.S. Sholl, *Density functional theory studies of sulfur binding on Pd, Cu and Ag and their alloys*, Surf. Sci. 546 (2003), pp. 12–26.
[13] A. Logadottir and J.K. Nørskov, *Ammonia synthesis over a Ru(0001) surface studied by density functional calculations*, J. Catal. 220 (2003), pp. 273–279.
[14] A. Soon, L. Wong, M. Lee, M. Todorova, B. Delley, and C. Stampfl, *Nitrogen adsorption and thin surface nitrides on Cu(111) from first-principles*, Surf. Sci. 601 (2007), pp. 4775–4785.
[15] C. Stampfl, S. Schwegmann, H. Over, M. Scheffler, and G. Ertl, *Structure and stability of a high-coverage (1×1) oxygen phase on Ru(0001)*, Phys. Rev. Lett. 77 (1996), pp. 3371–3374.
[16] S.H. Payne, J.-S. Mcewen, H.J. Kreuzer, and D. Menzel, *Adsorption and desorption of CO on Ru(0001): a comprehensive analysis*, Surf. Sci. 594 (2005), pp. 240–262.
[17] J.S. McEwen, S.H. Payne, H.J. Kreuzer, M. Kinne, R. Denecke, and H.-P. Steinrüuck, *Adsorption and desorption of CO on Pt(111): a comprehensive analysis*, Surf. Sci. 545 (2003), pp. 47–69.
[18] J.S. McEwen, S.H. Payne, and C. Stampfl, *Phase diagram of O/Ru(0001) from first principles*, Chem. Phys. Lett. 361 (2002), pp. 317–320.
[19] C. Stampfl, *Surface processes and phase transitions from* ab initio *atomistic thermodynamics and statistical mechanics*, Catal. Today 105 (2005), pp. 17–35.
[20] B.C. Han, A. Van der Ven, G. Ceder, and B.J. Hwang, *Surface segregation and ordering of alloy surfaces in the presence of adsorbates*, Phys. Rev. B 72 (2005), 205409.
[21] M.H.F. Sluiter and Y. Kawazoe, *Invariance of truncated cluster expansions for first-principles alloy thermodynamics*, Phys. Rev. B 71 (2005), 212201.
[22] G. Kresse and J. Furthmuller, *Efficiency of* ab-initio *total energy calculations for metals and semiconductors using a plane-wave basis set*, Comput. Mater. Sci. 6 (1996), pp. 15–50.

[23] G. Kresse and J. Furthmüller, *Efficient iterative schemes for* ab initio *total-energy calculations using a plane-wave basis set*, Phys. Rev. B 54 (1996), pp. 11169–11186.
[24] G. Kresse, J. Furthmüller, and J. Hafner, *Theory of the crystal-structures of selenium and tellurium – the effect of generalized-gradient corrections to the local-density approximation*, Phys. Rev. B 50 (1994), pp. 13181–13185.
[25] G. Kresse and J. Hafner, Ab initio *molecular-dynamics for liquid-metals*, Phys. Rev. B 47 (1993), pp. 558–561.
[26] P.E. Blöchl, *Projector augmented-wave method*, Phys. Rev. B 50 (1994), pp. 17953–17979.
[27] J.P. Perdew and Y. Wang, *Accurate and simple analytic representation of the electron-gas correlation-energy*, Phys. Rev. B 45 (1992), pp. 13244–13249.
[28] H.J. Monkhorst and J.D. Pack, *Special points for Brillouin-zone integrations*, Phys. Rev. B 13 (1976), pp. 5188–5192.
[29] J.M. Sanchez, F. Ducastelle, and D. Gratias, *Generalized cluster description of multicomponent systems*, Phys. A 128 (1984), pp. 334–350.
[30] G. Ceder, *A derivation of the Ising model for the computation of phase diagrams*, Comput. Mater. Sci. 1 (1993), pp. 144–150.